RESEARCH ARTICLE

Key Points:
- River sampling allows determining chemistry of groundwater discharge
- No assumption of groundwater end-member chemistry is required
- Bank storage water return can be partially identified

Supporting Information:
- Readme
- Figure S1, S2
- Table S1, S2

Correspondence to:
J. Batlle-Aguilar,
jordi.batlleaguilar@flinders.edu.au

Chemistry of groundwater discharge inferred from longitudinal river sampling

J. Batlle-Aguilar[1], G. A. Harrington[1,2,3], M. Leblanc[4], C. Welch[1], and P. G. Cook[1,2]

[1]National Centre for Groundwater Research and Training (NCGRT), School of the Environment, Flinders University, Adelaide, South Australia, Australia, [2]Water for a Healthy Country National Research Flagship, Commonwealth Scientific and Industrial Research Organization, Division of Land and Water, Adelaide, South Australia, Australia, [3]Innovative Groundwater Solutions, Blackwood, South Australia, Australia, [4]School of Earth and Environmental Sciences, National Centre for Groundwater Research and Training, James Cook University, Cairns, Queensland, Australia

Abstract We present an approach for identifying groundwater discharge chemistry and quantifying spatially distributed groundwater discharge into rivers based on longitudinal synoptic sampling and flow gauging of a river. The method is demonstrated using a 450 km reach of a tropical river in Australia. Results obtained from sampling for environmental tracers, major ions, and selected trace element chemistry were used to calibrate a steady state one-dimensional advective transport model of tracer distribution along the river. The model closely reproduced river discharge and environmental tracer and chemistry composition along the study length. It provided a detailed longitudinal profile of groundwater inflow chemistry and discharge rates, revealing that regional fractured mudstones in the central part of the catchment contributed up to 40% of all groundwater discharge. Detailed analysis of model calibration errors and modeled/measured groundwater ion ratios elucidated that groundwater discharging in the top of the catchment is a mixture of local groundwater and bank storage return flow, making the method potentially useful to differentiate between local and regional sourced groundwater discharge. As the error in tracer concentration induced by a flow event applies equally to any conservative tracer, we show that major ion ratios can still be resolved with minimal error when river samples are collected during transient flow conditions. The ability of the method to infer groundwater inflow chemistry from longitudinal river sampling is particularly attractive in remote areas where access to groundwater is limited or not possible, and for identification of actual fluxes of salts and/or specific contaminant sources.

1. Introduction

Perennial rivers are sustained by groundwater discharge during prolonged periods of low rainfall [*Séguis et al.*, 2011]. To maintain their ecological value for future generations, effective water management at the catchment scale is required. Effective water management involves quantifying groundwater discharge and also establishing the source and location of groundwater discharge into rivers. A number of studies have estimated rates of groundwater discharging into gaining rivers by comparing river and groundwater chemistry using a mass balance model [*Cook et al.*, 2006]. Recently, a few studies have also determined the relative contribution of different groundwater sources [*Gardner et al.*, 2011; *Harrington et al.*, 2013; *Opsahl et al.*, 2007]. Using the mass balance to obtain information about groundwater inflow into rivers generally assumes knowledge of the groundwater end-member chemistry [*Holtzman et al.*, 2005; *Meredith et al.*, 2009]. However, the assumption that the water chemistry measured in wells some distance from the river reflects that of groundwater flowing into the river might not always be valid. In other situations, even if the assumption is valid, access to groundwater in remote areas is often limited or not possible, thus accurate determination of end-member composition is difficult.

Inferring chemistry of groundwater inflow from synoptic river sampling has been used during the last decade in a range of small catchments. *Kimball et al.* [2001] found that stream water chemistry was controlled by the weathering of carbonate rocks and mine drainage inflows. *Barringer et al.* [2007] found that groundwater chemistry was responsible for temporal and spatial variations of arsenic concentration in a New Jersey watershed. Recently, *Banks and Palumbo-Roe* [2010] calculated the mass balance of inflow chemical loads in a mining area by synoptically sampling and flow gauging a tributary of the River Wear (UK). All of these studies deal with mine drainage inflows; this approach, however, has not yet been applied in combination

with environmental tracers to examine the chemistry of groundwater discharge and its potential relation to the catchment geology.

Tropical environments are sensitive ecosystems of rich biodiversity, which could potentially be threatened by major development and climate change impacts [*Webster et al.*, 2005]. The perennial rivers of northern Australia supply large volumes of fresh water, making them attractive prospects for new irrigation development, particularly to mitigate the impacts of recent drought and the longer term effects of climate change in southern Australia [*McGuire et al.*, 2005]. Increasing pressure on water supply and river systems elsewhere in Australia is driving strong interest in use of the abundant water resources in the north for agriculture [*Gehrke et al.*, 2004]. However, the vast area and remoteness of these tropical catchments limits research into the feasibility of these projects.

In the present study, we examine the potential to determine the chemistry of groundwater discharging into a river by synoptic river sampling. This technique has never been applied to river lengths greater than 100 km to our knowledge, whereas here we extend the technique to 450 km of river length. We make use of the river chemistry and a steady state one-dimensional advective transport model to infer the location and rate of groundwater discharge and inflow chemistry at a catchment scale, without a priori assumption of the groundwater end-member chemistry. The method we present does not intend to replace direct groundwater sampling, but to complement it. It is useful to determine snapshots of distributed fluxes of salts and/or specific contaminants, which when complemented with direct groundwater sampling, can achieve reliable results. It is particularly helpful in areas where access to groundwater is difficult or impossible (i.e., inaccessible remote areas), and might contribute to a reduction in costs associated with drilling of wells to explore groundwater resources.

2. Study Area

The Mitchell River catchment is located in tropical north Queensland, Australia, covering an area of >72,000 km^2 (Figure 1). The Mitchell River flows for a distance of approximately 600 km in a westerly direction from its headwaters in the Daintree Rainforest before discharging into the Gulf of Carpentaria. It has four main tributaries (from east to west): the Walsh, Lynd, Palmer, and Alice Rivers, and numerous smaller tributaries (creeks) in the upper catchment, the most important in terms of discharge being the Rifle, Mary, and McLeod Creeks. The study area covers a length of >400 km of the Mitchell River, from the headwaters to the confluence with the Palmer River.

The majority of the catchment is Dry Tropics savannah, with <20% of the area being Wet Tropics rainforest (in the upper, eastern part of the catchment). The area is generally remote and uninhabited, so direct river access is limited. Furthermore, the river is the habitat of both freshwater crocodile (*Crocodylus johnstoni*) and saltwater crocodile (*Crocodylus porosus*), making safe ground-based access to the river problematic.

2.1. Climate and Hydrology
In tropical northern Australia, the climate is characterized by two distinct seasons; on average about 90% of annual rainfall occurs in the "wet season" between November and March, with the remainder of the year classified as a "dry season." Mean annual rainfall for the region is 965 mm, although there is a strong east-west gradient reflected by the transition from upland rainforest in the headwaters (east), to the flat savannah landscapes in the west. There is high potential evapotranspiration during the dry season, from May to October (average of 5.2 mm d^{-1}). Several flow-gauging stations managed by the Queensland Department of Natural Resources and Mines (DNRM) (http://watermonitoring.derm.qld.gov.au/host.htm) are located along the Mitchell River and its tributaries (Figure 1). The Mitchell River has a marked seasonal flow regime, with high water levels and extensive flooding during the wet season and reduction of discharge and river stage toward the end of the dry season (Figure 2).

2.2. Geology and Hydrogeology
The Mitchell River flows across seven distinct geologic units. Within the upper 180 km, it flows through Silurian-Devonian marine sedimentary deposits including mudstones and graywackes (Hodgkinson Formation, HF). From 180 to 215 km downstream, the river crosses a mixture of Proterozoic-Paleozoic siliciclastic igneous-intrusive and metamorphic rocks. Outcrops of Jurassic sandstones (Gilbert River Formation, GRF)
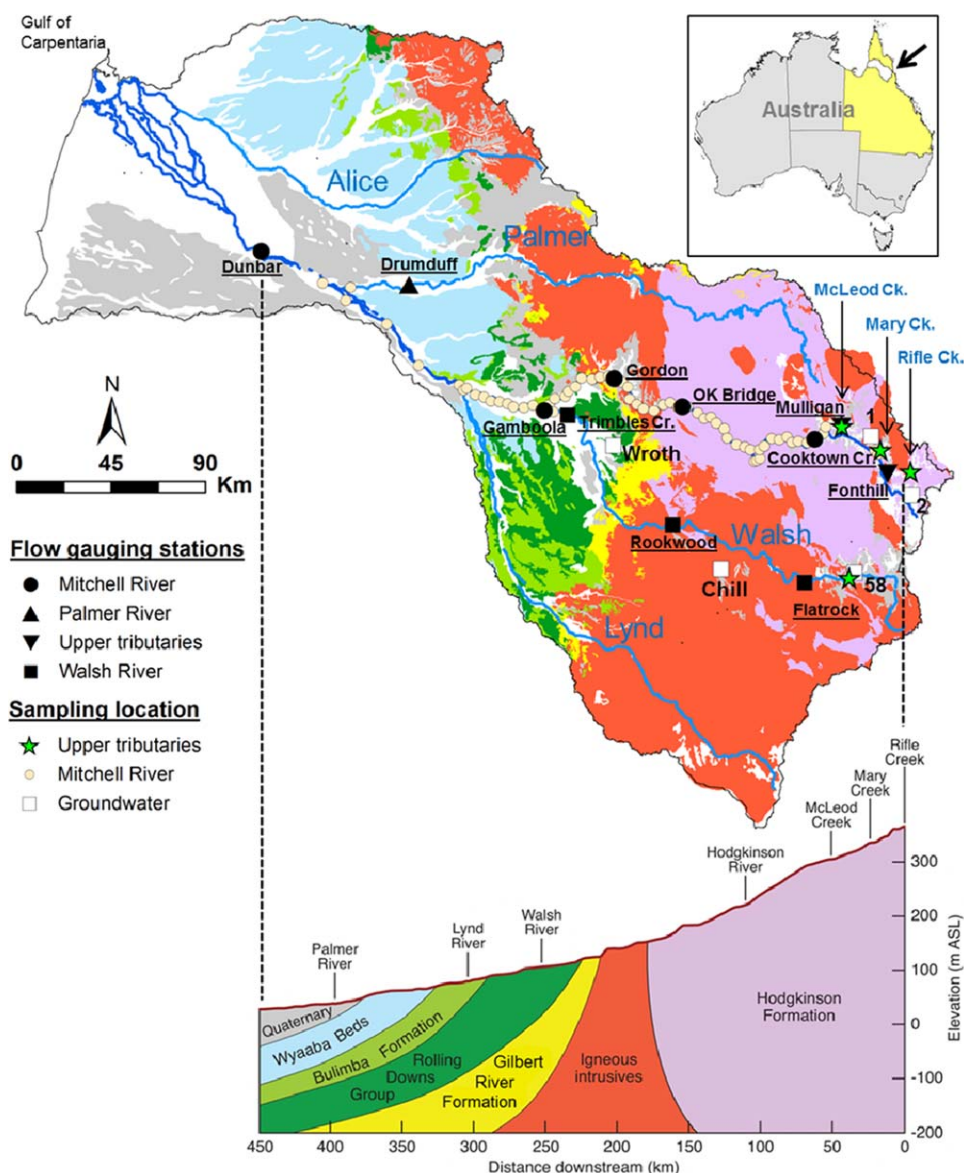
Figure 1. Surface geology and hydrography of the Mitchell River catchment. Flow gauging stations are shown with underlined names, sampling locations along the Mitchell River with yellow dots, upper tributaries sampling locations with green stars, and groundwater sampling locations with white squares. Geological cross section along the Mitchell River.

are found between 215 and 225 km, while heavily faulted early Cretaceous mudstones (Rolling Downs Group, RDG) are found from 225 to 295 km downstream. Oligocene sandstones (Bulimba Formation, BF) between 295 and 330 km, outcrop after the confluence of the Lynd River, followed by thick sequences of Miocene to Pliocene sandstones (Wyaaba Beds, WB) from 330 to 380 km, and Quaternary Alluvial Sediments (QAS) from 380 km onward, only a few meters above sea level (Figure 1).

Four main types of aquifers are found in the catchment: (I) fractured rock basement; (II) sandstones of the Great Artesian Basin (GAB); (III) Cenozoic sediments, and (IV) Quaternary alluvium. The fractured rock basement, comprising predominantly the HF, includes marine siliciclastic rocks and graywackes that constitute unconfined fractured rock aquifers with variable permeability and low storage, for which the mechanism of recharge is limited to direct rainfall [*CSIRO*, 2009]. As part of the GAB, Jurassic sandstones of the GRF outcrop in the center of the catchment in a north-south orientation; here the aquifer is unconfined. In the west, this aquifer is confined and artesian. The Oligocene sandstones of the BF is the most dominant formation of
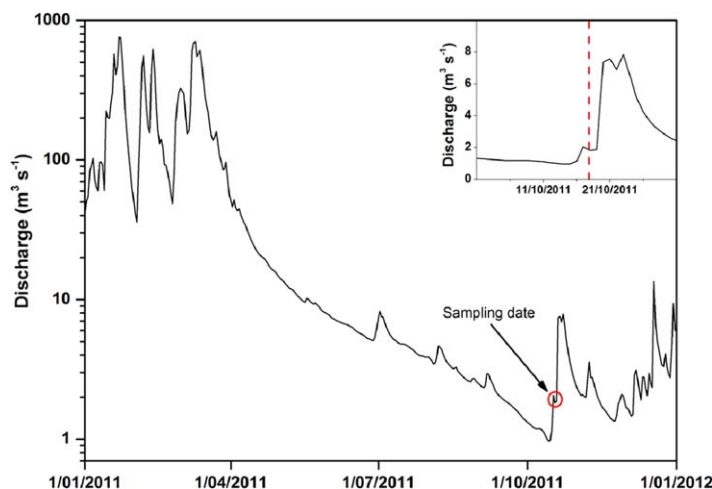
Figure 2. Mitchell River hydrograph of 2011 at the Cooktown Crossing automated flow gauging station (see location of gauging station in Figure 1). Inset: Hydrograph of October 2011 (the dashed red line shows the sampling day).

Cenozoic age in the area, and is composed of fluvial sediments derived from weathering of the GRF in the center of the catchment. Despite its high surface outcrop in the western part of the catchment, this formation is believed to be of limited productivity, as aquifers are mainly restricted to discontinuous meandering paleochannels. Finally, sediments deposited by the Mitchell River and its tributaries in occasional floods constitute the Quaternary aquifer, restricted to the western part of the catchment. Maintenance of river flows throughout the dry season is provided in part by runoff from the elevated rainforest at the top of the catchment, and in part by groundwater discharge (i.e., base flow).

3. Methodology

3.1. Tracers Used in This Study

Water chemistry measurements included radon activity, the strontium isotopic ratio and major and minor ion concentrations. Radon-222 (^{222}Rn) is a noble gas produced in the subsurface by the radioactive decay of radium-226 (^{226}Ra). It is a useful tracer to determine groundwater discharge to rivers [*Cook et al.*, 2003, 2006], as the activity of ^{222}Rn in the atmosphere is negligible. ^{226}Ra is present in all rocks, and thus ^{222}Rn accumulates in groundwater achieving secular equilibrium after approximately 2 weeks [*Ellins et al.*, 1990]. ^{222}Rn volatilizes to the atmosphere and has a short half-life (3.83 days). These factors make ^{222}Rn a useful tool to differentiate between sources of surface and subsurface water.

The strontium isotopic ratio (^{87}Sr/^{86}Sr) has been proven to be a useful tool to determine mixing of water of different origins [*Harrington and Herczeg*, 2003; *Semhi et al.*, 2000]. ^{87}Sr is the product of ^{87}Rb decay (half-life = 4.9×10^{10} years), which adds to the original amount of ^{87}Sr [*McNutt*, 1999]. Rocks and minerals with different Rb/Sr ratios will therefore develop a specific ^{87}Sr/^{86}Sr ratio, which will determine different ratios for Sr dissolved in water due to rock weathering [*Blum et al.*, 1993]. For example, marine carbonates typically have ratios of about 0.709, reflecting that of Phanerozoic seawater [*Burke et al.*, 1982], whereas silicate rocks have much higher values, often higher than 0.750. That said, a range of Sr isotopic ratios can be produced during weathering reflecting the Sr isotopic ratio of constituent minerals [*Petelet-Giraud et al.*, 2003]. This ratio cannot be used as an indicator of water age, as rocks with the same Rb/Sr can have different ages. Relationships between ^{87}Sr/^{86}Sr and Sr^{2+}, Cl$^-$, SO$_4^{2-}$ and other cations/anions can be used to constrain natural and/or anthropogenic contamination, as well as mixing between surface and groundwater [*Petelet-Giraud et al.*, 2007].

The major ion chemistry of groundwater discharge to a river is the result of mineral dissolution and rock weathering reactions in the host aquifer as well as redox processes, dissolution and precipitation salts in soils and biological uptake (e.g., vegetation), particularly for shallow aquifers. In relatively small catchments (e.g., hundreds of square kilometers), the effects of processes other than rock weathering on groundwater chemistry have been shown to be important [*Négrel and Deschamps*, 1996]. In contrast, rock weathering of the aquifer matrix can explain up to 90% of the water chemistry in large, regional catchments (e.g., tens of thousands of square kilometers [*Négrel and Lachassagne*, 2000; *Petelet et al.*, 1998; *Reeder et al.*, 1972; *Stallard and Edmond*, 1983]). Therefore, changes in geology are expected to play a major role in the chemistry of groundwater discharge along the Mitchell River.
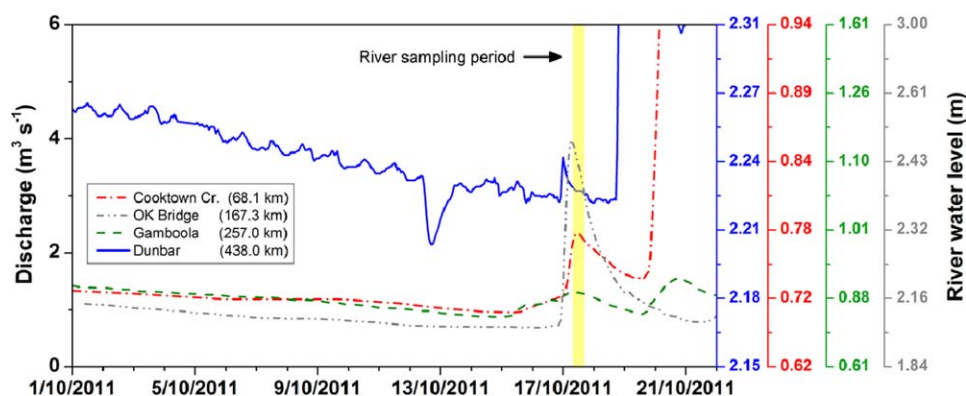
Figure 3. Hydrographs for all the available automatic flow gauging stations along the studied 450 km of the Mitchell River for October 2011. The yellow vertical bar highlights the sampling period with the helicopter on 17 October, from 8 am to 4 pm.

3.2. Surface and Groundwater Sampling

Surface water and groundwater in the Mitchell River catchment were sampled at the end of the dry season in October 2011. The sampling program was conducted in three parts across the upper 400 km of the catchment (Figure 1).

Part 1 consisted of high-resolution river sampling conducted by helicopter on a single day (17 October 2011). This procedure not only maximized the likelihood of capturing a particular snapshot in time of the flow conditions along the studied reach, but also overcame access difficulties due to the remoteness of the area and the abundance of saltwater crocodiles (*Crocodylus porosus*). Unfortunately, a small flow event occurred the day before sampling due to scattered rainfall in the upper part of the catchment (Figure 3). Sampling locations were distributed every 5 km along the reach from 68 to 309 km downstream, and every 25 km between 309 and 393 km. Coordinates of these sampling locations were uploaded to the helicopter's GPS. Samples were collected by hovering the helicopter over the river and directly sampling with a submersible pump attached to a marine buoy following the methods of *Gardner et al.* [2011] and *Harrington et al.* [2013]. All 60 samples collected were analyzed for major ions, ^{222}Rn and the ^{87}Sr/^{86}Sr ratio.

Part 2 consisted of sampling at two points on the upper Mitchell River and four of its tributaries (Rifle, Mary, and McLeod Creeks, and Walsh River) where access with helicopter was not possible due to dense vegetation. These sites were sampled via vehicle access on the following day (18 October 2011). These sampling points covered the remaining 68 km of the upper part of the catchment. As well as sample collection for analysis of major ions, ^{222}Rn and ^{87}Sr/^{86}Sr ratio, field measurements of pH, EC, and temperature were performed.

Part 3 consisted of sampling five regional wells and monitoring piezometers in contrasting geologic units using a 12 V submersible pump on 18–19 October 2011 (Figure 1). Samples were collected for the analysis of major ions, ^{87}Sr/^{86}Sr ratio and ^{222}Rn, and field measurements of pH, EC, and temperature were performed. Remoteness and isolation of the area made it impossible to sample wells located closer to the river.

Water for major ion chemistry was collected in 125 mL polyethylene bottles, filtered (0.45 μm) and, for cations, acidified with concentrated HNO_3^- in the field. Samples for ^{222}Rn were collected following the polyethylene terephthalate (PET) bottle method [*Leaney and Herczeg*, 2006] and sent to the laboratory the day after they were collected. Samples for ^{87}Sr/^{86}Sr were collected in 0.5 L polyethylene bottles.

3.3. Analytical Methods

Field temperature, EC (±0.5% accuracy), and pH (±0.004 accuracy) measurements were performed with a WTW Multimeter 3420 Set, while DO measurements were performed using a Hydrolab DS5X (0.01 mg L^{-1} resolution, ±0.1 mg L^{-1} accuracy). Major ion analyzes were performed by Inductively Coupled Plasma Mass Spectrometry (ICP-MS) at the Commonwealth Scientific and Industrial Research Organisation (CSIRO) Analytical Chemistry Unit in Adelaide (Australia). ^{222}Rn samples were analyzed 2 days after sampling at the CSIRO Isotope Analysis Service (IAS) in Adelaide, using low-level liquid scintillation counting with α/β separation [*Leaney and Herczeg*, 2006]. The detection limit of the method is $\sim$ 3 mBq L^{-1}, and the 1σ analytical error

Table 1. Measured Discharge Flows of the Mitchell River and Main Tributaries Before and During the Two Sampling Days in October 2011[a]

Flow Gauging Station	River	Dist. Downstream (km)	Latitude	Longitude	Gauging Time	Discharge (m³ s⁻¹)				
						15 October 2011	17 October 2011	18 October 2011		
						DNRM	DNRM	DNRM	ADCP	FLO-MATE™
Fonthill	Rifle Ck.	0.0	−16.6809	145.2262	15:00	0.282	0.557	0.512	–	–
Upstream Mary	Mitchell Rv.	25.3	−16.6013	145.1741	12:20	n.a.	n.a.	n.a.	–	0.562
Mary	Mary Ck.	26.5	−16.5838	145.1833	11:00	n.a.	n.a.	n.a.	–	0.309
Mulligan	McLeod Ck.	56.0	−16.5838	145.1833	15:00	0.626	1.456	0.998	–	1.041
Cooktown Crossing	Mitchell Rv.	68.1	−16.5630	144.8886	15:00	0.956	2.268	1.768	–	–
OK Bridge	Mitchell Rv.	167.3	−16.4710	144.2892	14:00	0.695	3.306	1.634	–	–
Gordon Arnold Crossing	Mitchell Rv.	208.5	−16.3748	143.9768	10:50	n.a.	n.a.	n.a.	0.572	–
Trimbles Crossing	Walsh Rv.	256.2	−16.5479	143.7835	11:00	0.582	0.712	0.214	0.275	–
Gamboola	Mitchell Rv.	257.0	−16.5349	143.6775	12:00	0.983	1.299	1.086	–	–
Upstream Lynd	Mitchell Rv.	306.7	−16.4636	143.3102	15:35	n.a.	n.a.	n.a.	2.712	–
Lynd	Lynd Rv.	308.6	−16.4661	143.3079	15:10	n.a.	n.a.	n.a.	3.17	–
Downstream Lynd	Mitchell Rv.	310.6	−16.4606	143.3064	16:00	n.a.	n.a.	n.a.	5.932	–
Drumduff	Palmer Rv.	393.1	−16.0401	143.0379	08:00	0.585	0.936	1.299	–	–
Dunbar	Mitchell Rv.	438.0	−15.9411	142.3742	08:00	3.143	3.218	3.143	–	–

[a]DNRM, discharge values obtained from gauging stations of the Department of Natural Resource and Mines (http://watermonitoring.derm.qld.gov.au/host.htm); ADCP, flow discharge measured using an Acoustic Doppler Current Profiler; FLO-MATE™, flow discharge measured using a portable flowmeter; n.a., DNRM flow gauging station not available. Gauging times correspond to approximately the moment we were sampling nearby with the helicopter. Shaded values were used during modeling.

was ∼10.2%. ^{87}Sr/^{86}Sr was analyzed at the University of Adelaide, Mawson Laboratories, using a Finnigan MAT 262 thermal ionization mass spectrometer. All ^{87}Sr/^{86}Sr ratios were normalized to a NBS 987 ^{87}Sr/^{86}Sr ratio of 0.710229. Sr concentrations, used to infer the modeled ^{87}Sr/^{86}Sr ratio of groundwater discharge, had a detection limit of 0.05 mg L^{-1}.

3.4. Surface Water Discharge

During the sampling period, the Mitchell River was flow gauged at eight locations along the studied reach (Table 1 and Figure 1). All tributaries were also gauged, with the exception of the Hodgkinson River (no access). Flow gauging was performed the same day as the helicopter sampling or the following day. An Acoustic Doppler Current Profiler (ADCP) or a FLO-MATE^{TM} 2000 portable electromagnetic flowmeter was used, and for those locations where access was not possible, discharge values were obtained from automated flow gauging stations of the Queensland Department of Natural Resources and Mines (DNRM) (http://watermonitoring.derm.qld.gov.au/host.htm).

3.5. Modeling

3.5.1. One Dimensional Advective Transport Model

Changes in flow, tracer composition, and chemical concentration in the river were modeled using a 1-D advective transport model that takes into account groundwater inflow into the river, losses of water from the river and, for ^{222}Rn, atmospheric exchange, production within the hyporheic zone, and decay within the river and the hyporheic zone. The change in flow with distance in the river is given by

$$\frac{\partial Q}{\partial x} = I - wE - L, \tag{1}$$

where Q is the river discharge (m³ d⁻¹), x is the distance in the flow direction (m), I is the groundwater inflow rate per unit of river length (m³ d⁻¹ m⁻¹), E is the evaporation rate (m d⁻¹), w is the average width of the river surface (m), and L is the loss rate per unit length (m³ d⁻¹ m⁻¹). The loss rate represents either water pumped out of the river system (e.g., water used for irrigation, livestock, and human consumption) or losses to the underlying aquifer. The Mitchell River catchment is remote and extremely sparsely populated, hence, pumping from the river may be assumed to be negligible.

Table 2. Model Parameterization

Parameter	Symbol	Value	Units
Total river length	x	450	km
Average river width	w	10–20	m
Mean river depth	d	1–0.5	m
Evaporation rate	E	5	mm d^{-1}
Initial river discharge	Q_o	25,920 (0.3)	m^3 d^{-1} (m^3 s^{-1})
Hyporheic porosity	θ	0.4	–
Mean hyporheic depth	h	1.0	m
Hyporheic residence time	t_h	0.25	d
^{222}Rn Hyporheic production rate	γ	0.2	Bq L^{-1} d^{-1}
^{222}Rn decay coefficient	λ	0.181	d^{-1}
^{222}Rn transfer velocity	k	1.6	m d^{-1}
^{222}Rn initial activity	$^{222Rn}C_{i_{sw}}$	0.34	Bq L^{-1}
EC initial conc.	$^{EC}C_{i_{sw}}$	80.0	μS cm^{-1}
Sr* initial conc.	$^{Sr*}C_{i_{sw}}$	0.02	mg L^{-1}
Na$^+$ initial conc.	$^{Na}C_{i_{sw}}$	8.5	mg L^{-1}
K$^+$ initial conc.	$^{K}C_{i_{sw}}$	1.2	mg L^{-1}
Mg^{2+} initial conc.	$^{Mg}C_{i_{sw}}$	1.0	mg L^{-1}
Ca^{2+} initial conc.	$^{Ca}C_{i_{sw}}$	8.6	mg L^{-1}
Si^{2+} initial conc.	$^{Si}C_{i_{sw}}$	8.0	mg L^{-1}
SO$_4^{2-}$ initial conc.	$^{SO_4^{2-}}C_{i_{sw}}$	1.5	mg L^{-1}
HCO$_3^-$ initial conc.	$^{HCO_3^-}C_{i_{sw}}$	15.0	mg L^{-1}
Cl$^-$ initial conc.	$^{Cl}C_{i_{sw}}$	14.0	mg L^{-1}

Tracer concentration change along a river that receives groundwater inflow is given by [*Cook et al.*, 2006]:

$$Q\frac{\partial Q}{\partial x} = I_{gw}\left(c_{i_{gw}} - c\right) - I_{sw}\left(c_{i_{sw}} - c\right) + wEc - kw(c - Sc_a) - \lambda dwc + \frac{\lambda hw\theta}{1 + \lambda t_h}(1 - c), \qquad (2)$$

where c is the concentration of a given tracer in the river, c_i is the concentration of the same tracer in the water inflow, k is the gas transfer velocity across the water surface (m d^{-1}), S is the tracer solubility, c_a is the atmospheric mixing ratio for gaseous tracers (-), λ is the radioactive decay constant (d^{-1}), d is the mean river depth (m), γ is the hyporheic production rate (Bq L^{-1} d^{-1}), h is the mean hyporheic depth (m), t_h is the mean residence time of water in the hyporheic zone (d), and θ is the hyporheic zone porosity (-). Subscripts "*gw*" and "*sw*" in the I term refer to groundwater and surface water inflow, respectively. Terms 1 to 6 in the right-hand side of equation (2) represent changes in river concentration due to groundwater inflow, surface water from tributaries, evaporation, gas exchange, radioactive decay within the river and production and radioactive decay within the hyporheic zone. In this study, terms 5 and 6 only apply to ^{222}Rn. This modeling approach assumes steady state discharge in a river which in reality rarely occurs. In order to approximate steady state under transient conditions river samples are required to be collected in a very short period of time. An analysis of the consequences on estimating groundwater discharge and its chemistry when applying a steady state model under transient river flow conditions is presented in Appendix A.

3.5.2. Model Parameterization

Model parameters and initial values are presented in Table 2. Based on field measurements during river flow gauging, the river width (w) was fixed to 10 m in the upper catchment, where the river is relatively well channelled, and linearly interpolated downstream to 20 m width at the end of the reach studied ($x = 450$ km), where the flood plains are wider and the river becomes more braided. Although the river was only sampled for 400 km, the model domain was extended to 450 km where the Dunbar flow gauging station is located, as it provides a downstream boundary condition. Based on field observations, the river depth (d) was interpolated from 1 m in the upper catchment to 0.5 m at the downstream end. An evaporation rate (E) of 5 mm d^{-1} was assigned, consistent with that used in previous studies of northern Australia [*Gardner et al.*, 2011; *Smerdon et al.*, 2012]. An initial upstream river discharge (Q_o) of 25,920 m^3 d^{-1} (0.3 m^3 s^{-1}) was assigned based on flow measurements carried out in the upper catchment. Hyporheic porosity (θ), depth (h), and residence time (t_h) were assumed constant with 0.4, 1 m, and 0.25 days, respectively [*Gardner et al.*, 2011]. *Harrington et al.* [2013] showed that model sensitivity to these parameters is as low as 0.01 for a similar river in northern Australia (i.e., 100% variation on the parameter induces a change in model output of

1%). A ^{222}Rn exchange velocity (k) of 1.6 m d^{-1} and hyporheic production rate (γ) of 0.2 Bq L^{-1} were assumed based on previous studies done in similar riverine environments [*Gardner et al.*, 2011]. The ^{222}Rn decay coefficient (λ) is 0.181 d^{-1}. The product of Sr^{2+} concentration and ^{87}Sr/^{86}Sr ratio, labeled herein as Sr*, was modeled instead of the ^{87}Sr/^{86}Sr ratio alone to ensure mass balance [*Harrington et al.*, 2013; *Semhi et al.*, 2000]. Initial EC $\left(^{EC}C_{i_{sw}}\right)$ values and tracer concentrations of ^{222}Rn $\left(^{222Rn}C_{i_{sw}}\right)$ and Sr* $\left(^{Sr^*}C_{i_{sw}}\right)$, were assigned to 80 μS cm^{-1}, 0.34 Bq L^{-1}, and 0.02 mg L^{-1}, respectively, based on surface water analysis in the upper catchment. The same approach was used to assign initial concentrations of major ions.

The measured discharge and chemistry of tributaries (Rifle, Mary, and McLeod Creeks, and Hodgkinson, Walsh, Lynd, and Palmer Rivers) were used as known input data to compute the flow and tracer mass balance.

Due to the sheer size of the Mitchell River catchment ($> 72{,}000$ km^2) and therefore the likely importance of geology as a control on the chemistry of groundwater discharge—either directly via weathering of aquifer minerals or indirectly via soil processes—we assumed a single flow-weighted chemistry for each geologic unit (Figure 1).

The modeling approach was to simulate measured river discharge and chemistry, and in doing so to estimate 14 different parameters: the rate and distribution of river loss (L) and groundwater discharge (I), and the chemistry of groundwater discharge including groundwater discharge ^{222}Rn activity, EC, and major ion (Na$^+$, Ca^{2+}, K$^+$, Mg^{2+}, Si^{2+}, Cl$^-$, SO$_4^{2-}$, HCO$_3^-$, Sr^{2+}) concentrations and Sr*. For locations in the river where measured Sr^{2+} concentrations were below the detection limit (0.05 mg L^{-1}), a half detection limit concentration of 0.025 mg L^{-1} was assumed.

The location and rate of groundwater discharge were anticipated to be highly variable along the river, thus the number of zones for groundwater discharge (I) and their rate were established through iteration designed to minimize the root mean square error (RMSE) of the modeled and measured Mitchell River discharge on the calibration output. A total of 44 discharge zones, of variable length, were allocated along the 450 km river length.

3.5.3. Model Calibration

Equations (1) and (2) were coded in Fortran in order to automate the calibration process and undertake uncertainty analysis of groundwater discharge and its chemistry using the automated parameter estimation code PEST [*Doherty*, 2008]. PEST uses a Gauss-Marquardt-Levenberg (GML) algorithm to minimize an objective function composed of the sum of weighted squared differences between model-generated outcomes and their corresponding field-measured counterparts. The objective function is defined as

$$\phi(u) = \sum_{i=1}^{n} w_i [o_i - m_i(u)]^2, \qquad (3)$$

where u is a vector containing values of each of the parameters being estimated, n is the number of observations, o_i is the i'th observation, m_i is the corresponding ith modeled observation, and w_i is the associated weight of the ith observation. Model calibration results in the best estimate of the modeled parameter and its 95% confidence interval.

PEST was implemented using the automatic user intervention option "auid" [*Doherty*, 2008]. This setting allows PEST to temporarily remove apparent excessively sensitive parameters from the parameter-estimation process, which contributes to lowering of the objective function.

3.5.4. Parameter Identifiability

The identifiability (f) of a parameter is a qualitative statistic that represents the capacity of the model to reliably identify a parameter with the available observations [*Doherty and Hunt*, 2010]. In order to calculate the identifiability of a parameter, the sensitivity of each model parameter to each model output for which field observations are available must first be calculated. The Jacobian matrix (X) is the finite difference approximation of the sensitivity matrix [*Doherty and Hunt*, 2009]. It consists of sensitivities of all specified model outputs to all adjustable model parameters and is computed through perturbation of an optimal parameter set. Singular Value Decomposition (SVD) is a technique that can be performed on the Jacobian matrix to divide the parameter space into calibration and null space [*Peeters et al.*, 2011]:
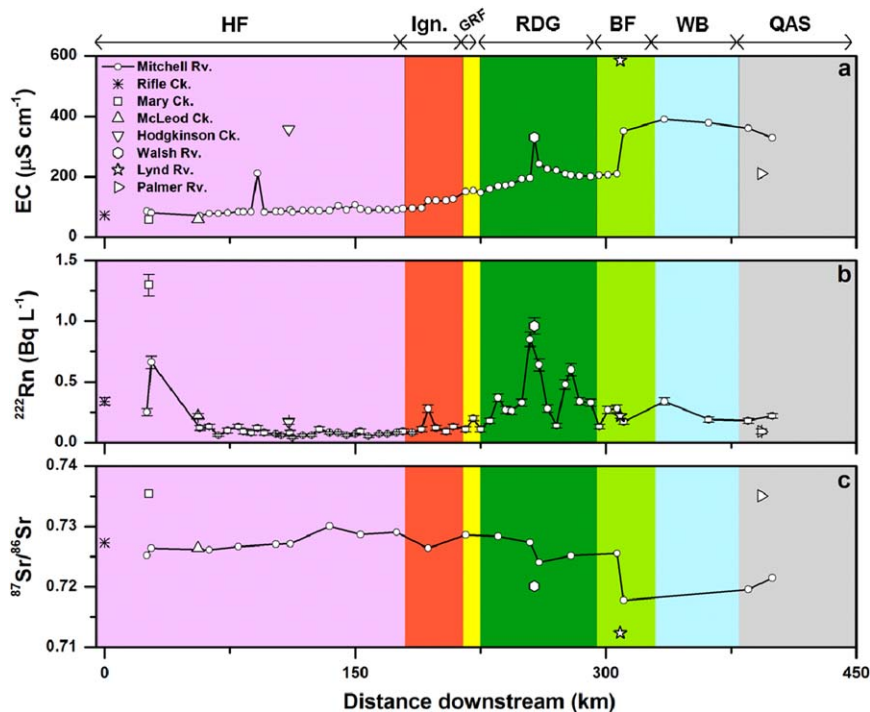
Figure 4. Sampling results along the Mitchell River and tributaries: (a) EC, (b) ^{222}Rn, and (c) ^{87}Sr/^{86}Sr ratio. Geology along the river is shown in background (HF, Hodgkinson Formation—Devonian graywacke; Ign, igneous and intrusive rocks; GRF, Gilbert River Formation—Jurassic sandstone; RDG, Rolling Downs Group—Cretaceous mudstone; BF, Bulimba Formation—Cenozoic sandstone; WB, Wyaaba Beds—Cenozoic sandstone; QAS, Quaternary—Cenozoic alluvium sediments).

$$Q^{1/2}X = USV^t, \tag{4}$$

where Q is the observation weight matrix, X is the Jacobian matrix, U is an orthogonal matrix spanning observation space, S is a diagonal matrix containing the singular values in decreasing order, and V^t is the transpose of an orthogonal matrix spanning parameter space.

SVD essentially creates weighted parameter combinations (V^t) that are themselves weighted based on the extent to which they are able to represent the variance present in the data (magnitude of singular values). In this way, parameter space is divided into calibration solution space (parameter combinations that will influence calibration so may be identified from the available data to some extent) and calibration null space (parameters do not influence calibration and hence cannot be identified from the available data).

Mathematically, identifiability is defined as [*Doherty and Hunt*, 2009]:

$$f_i = (VV^t)_{i,i}. \tag{5}$$

In simple terms, parameter identifiability f_i can be considered as the projection of parameter *i* on the calibration space: if $f_i = 1$, the parameter combination can be uniquely estimated, if $f_i = 0$ the observation data provides no information about the parameter combination, and where $0 < f_i < 1$, the parameter combination can be partly estimated. Identifiability was calculated via postcalibration analysis using the driver program GENLINPRED "general linear predictive uncertainty/error analyzer" within PEST [*Doherty*, 2008].

4. Results

4.1. Surface Water Chemistry

Results of EC, ^{222}Rn, and ^{87}Sr/^{86}Sr analyzes are presented in Figure 4 and Table S1. EC values are low (~60 μS cm^{-1}) along the upstream section of the Mitchell River (0–180 km), increasing from the Ign formation outcrops to reach its maximum (391 μS cm^{-1}) at 320 km downstream, where the WB formation outcrops. Low
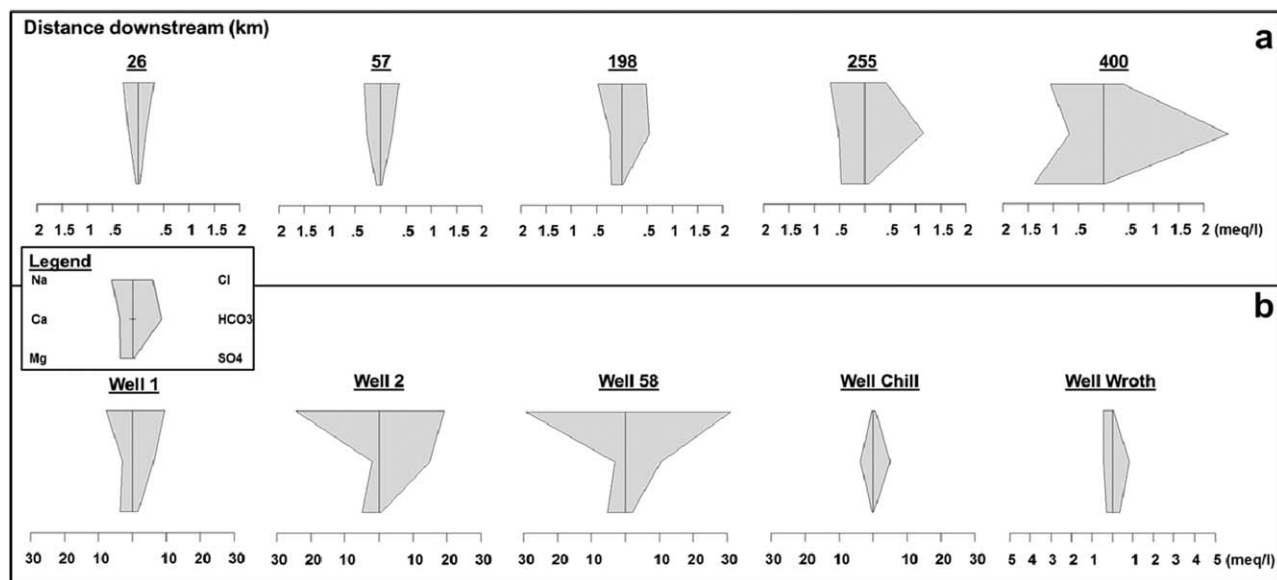
Figure 5. Stiff plots for (a) Mitchell River (numbers indicate distance downstream in km) and (b) groundwater samples (note the exaggeration in the concentration scale for Well Wroth).

^{222}Rn concentrations (<0.25 Bq L^{-1}) were observed in the Mitchell River while flowing across HF, Ign, and GRF formations (first 225 km), except for a local increase associated with inflow from Mary Creek. ^{222}Rn concentrations increased up to 0.85 Bq L^{-1} before the confluence with the Walsh River, at 254 km distance, in the RDG formation. For the last 150 km, where the Mitchell River flows across the BF, WB, and QAS formations, ^{222}Rn concentrations are similar to those observed in the upper catchment. Relatively high ^{87}Sr/^{86}Sr ratios of 0.72523–0.73006 were found during the first 250 km (approximately until the confluence with the Walsh River), decreasing to 0.717745 after the confluence with the Lynd River (Figure 4). ^{87}Sr/^{86}Sr ratios are generally consistent with the geologic units from which the tributaries originate; that is, lower values for the Lynd River (0.712360) reflect predominantly carbonate/mudstone rocks of the RDG, even though the upper part of that river catchment is in igneous rocks. Higher values for Mary Creek (0.735458) and Palmer River (0.735039) reflect the granitic geologies in their upper catchment or source area (Figure 1).

High relative proportions of Na$^+$ and Cl$^-$ characterize major ion chemistry of the uppermost catchment, while further downstream the surface water of the Mitchell River becomes more Mg^{2+} and HCO$_3^-$ dominated (Figure 5a and Table S2). Overall, the Mitchell River waters have very low levels of SO$_4^{2-}$.

4.2. Groundwater Chemistry

Results from wells 1, 2, and 58 indicate that groundwater chemistry in this part of the catchment is more dominated by Na$^+$, Cl$^-$, and HCO$_3^-$ in comparison to surface water (Figure 5b). Well 1 is located 37 km downstream of well 2, with both relatively close to the Mitchell River (5.6 and 4 km orthogonal distance, respectively) in the uppermost part of the catchment (Figure 1). Well 58 is completed in the same geologic unit (Hodgkinson Formation—HF), and located in the upper part of the Walsh River catchment, approximately 200 km upstream of the confluence with the Mitchell River. Although these wells are completed in the HF, their screens (6 m length) are all located at different levels: 40, 20, and 25 m below ground level for wells 1, 2, and 58, respectively. Vertical stratification within this formation may explain the variation in concentrations, although different spatial location in the aquifer may also explain these variations. Ca^{2+} and HCO$_3^-$ dominate the groundwater chemistry of Well Chill, which is consistent with the local occurrence of altered carbonate rocks (i.e., marble). The groundwater chemistry of Well Wroth has a distinct anionic composition, with high HCO$_3^-$ and SO$_4^{2-}$ relative to Cl$^-$. None of the cations are particularly dominant.

4.3. River Flow and Tracer Discharge

Measured river discharges during the sampling period are summarized in Table 1. FLO-MATE^{TM} and DNRM automated flow-gauging station values compared reasonably well at the single location where both types

of measurements are available (Mulligan gauging station on 18 October 2011). Significant differences were observed when comparing ADCP and DNRM sourced values (see for example Trimbles Crossing gauging station on 18 October 2011). However, flows in the order of 0.2 m^3 s^{-1} for the Walsh River are very low, making flow measurements prone to error in these conditions.

Discharge measurements in the Mitchell River during the second sampling day (18 October 2011) were 10–20% lower than the first sampling day (17 October 2011), with the exception of the flow gauging station of OK Bridge, where river discharge decreased by up to 50%. A local rainfall event on the 15 October in that area created a local flow event, the measurable increase in flow being mostly limited to the reach between Cooktown Crossing (68.1 km) and OK Bridge (167.3 km) gauging stations. The impact of that local flow event on river chemistry and resulting estimates of groundwater discharge and its chemistry is discussed in detail in Appendix A.

Analysis of the Mitchell River flow and tracer discharge during 17 October 2011 (only DNRM gauging stations) and 18 October 2011 (flow gauged values using either ADCP or FLO-MATE^{TM}) reveals that tributaries can only partially explain the increases in flow and tracer discharge along the Mitchell River (Figure S1). The uppermost tributaries of the catchment (Mary and McLeod Creeks) contribute up to 80% and 70% of the increases in flow and tracer discharge of the Mitchell River, respectively, whereas the contribution of Hodgkinson River is limited to 43% and 60%, respectively. Further downstream, the Walsh and Lynd Rivers contribute almost 100% of the increase in river tracer and flow discharge. However, between these two rivers (260–309 km distance downstream), there are no tributaries to explain the 109% and 81% increase in Mitchell River flow and tracer discharge, respectively, these increases being totally due to groundwater discharge.

4.4. Model Calibration Results

Calibrated river flow, tracer (EC, ^{222}Rn, and Sr) and major ion concentrations are shown in Figure 6 (left). The model was able to accurately reproduce the Mitchell River discharge during the sampling period 17–18 October 2011 and the general trend of tracer concentrations, with correlation coefficients ranging from 0.804 (^{222}Rn) to 0.985 (EC). The only exception was Cl, for which a correlation coefficient of 0.552 was obtained, possibly indicating some additional input from atmospheric deposition or surface water evaporation. Despite the low correlation coefficient, the general downstream trend is well captured. River loss via infiltration was found to occur in two areas of the studied reach, at around 176 and 380 km downstream, with fluxes of 2.8 × 10^5 and 3.3 × 10^5 m^3 d^{-1}, respectively.

Most of the ^{222}Rn activities were well captured by the model, notably those peaks between 250 and 300 km downstream, and the trend of EC increasing downstream (Figure 6, left). The model was able to reproduce the increasing trend in Sr after 225 km (Figure 6, left).

Model calibration using 44 individual reaches along the Mitchell River resulted in a detailed longitudinal profile of groundwater discharge rates (Figure 6, right). The reach where the Rolling Downs Group (RDG) outcrops was found to contribute the most groundwater discharge into the Mitchell River, with 2195 m^3 d^{-1} km^{-1} (1.5 × 10^5 m^3 d^{-1}). This reach is located between Gamboola gauging station and the Lynd River, a section with no tributaries. Although it only accounts for 15% of the length of the river, groundwater discharge within this reach corresponds to 40% of the total groundwater discharge into the Mitchell River. The area where the Hodgkinson Formation (HF) outcrops is the second most important reach in terms of groundwater discharge (24%), with a contribution of 508 m^3 d^{-1} km^{-1} (9.1 × 10^4 m^3 d^{-1}). The river reach receiving the smallest groundwater discharge (1.6%) corresponds to the Gilbert River Formation (GRF), with only 617 m^3 d^{-1} km^{-1} (6.2 × 10^3 m^3 d^{-1}). Reaches of Wyaaba Beds (WB), Igneous-intrusive rocks (Ign), Quaternary Alluvial Sediments (QAS) and Bulimba Formation (BF) contribute with 1187, 790, 352, and 530 m^3 d^{-1} km^{-1}, respectively (5.9, 2.8, 2.5, and 1.9 × 10^4 m^3 d^{-1}, respectively). The difference between measured and modeled river flow was 9%, with the modeled river flow being slightly overestimated in particular at two locations, Gamboola (257 km downstream) and Dunbar (438 km downstream) (Figure 6, left).

4.5. Groundwater Discharge Chemistry

Model calibration resulted in a longitudinal groundwater chemistry profile for each tracer (Figure 6, right). Modeled ^{222}Rn activities of groundwater discharging into the upper reaches of the Mitchell River were generally low (1.9–2.5 Bq L^{-1}), increasing to a maximum of up to 8.0 Bq L^{-1} in the area where the river flows across the Wyaaba Beds (WB). Modeled groundwater discharge EC varies between 100 and 350 μS cm^{-1}, with values generally increasing downstream. Modeled groundwater discharge ^{87}Sr/^{86}Sr ratio was found to
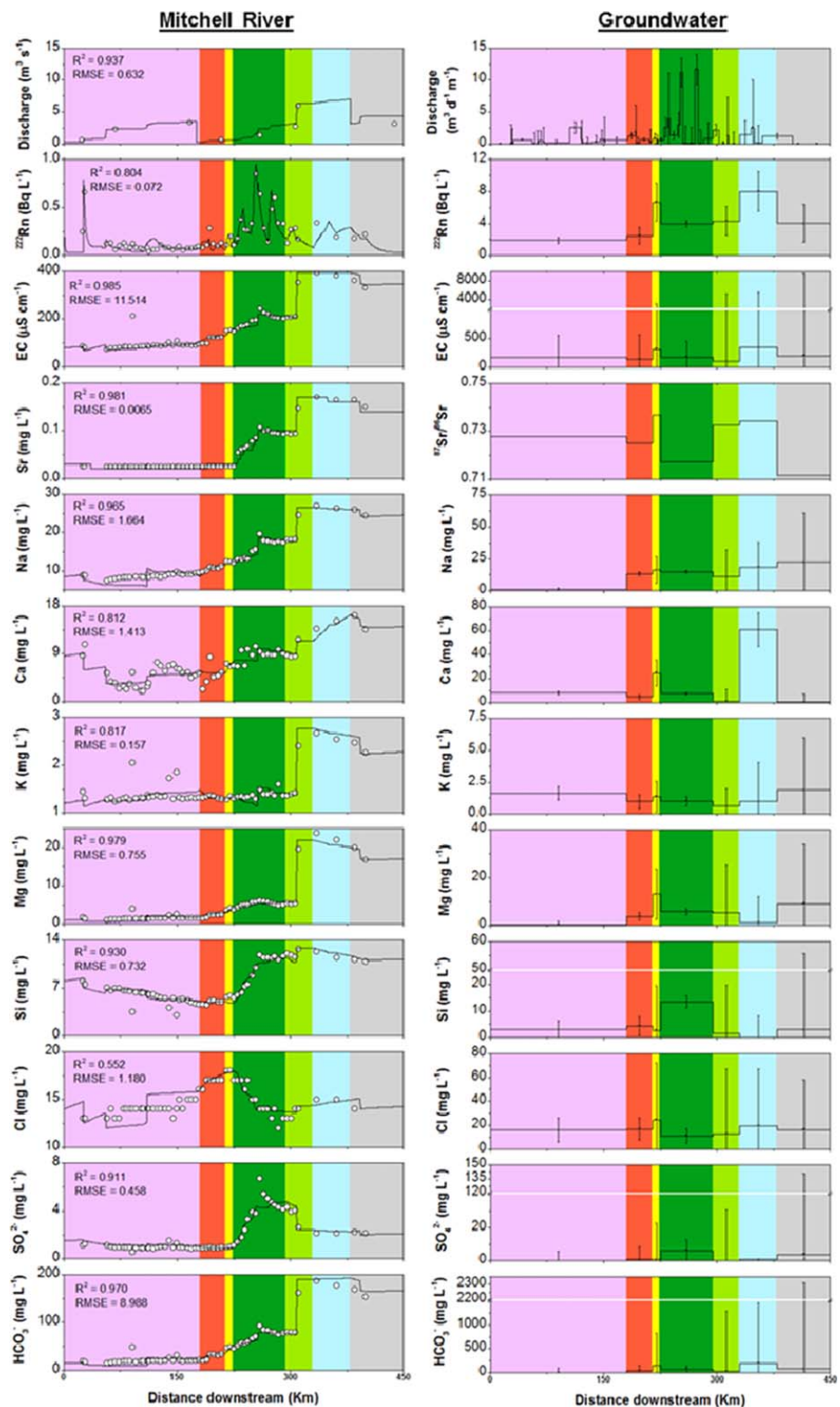
Figure 6. (left) Comparison of observed (hollow circles) and modeled (solid line) parameters. (right) Modeled groundwater discharge rate and chemical composition of groundwater discharging along 450 km of the Mitchell River. Modeled error bars represent the 95% confidence interval for the estimated value from PEST, highlighting reliability of the estimated value.

vary between 0.73684 and 0.71153, although no particular trend was observed. Regarding modeled groundwater chemistry, groundwater discharging in the upper part of the catchment (0–210 km) had comparatively lower concentrations than the lower catchment.
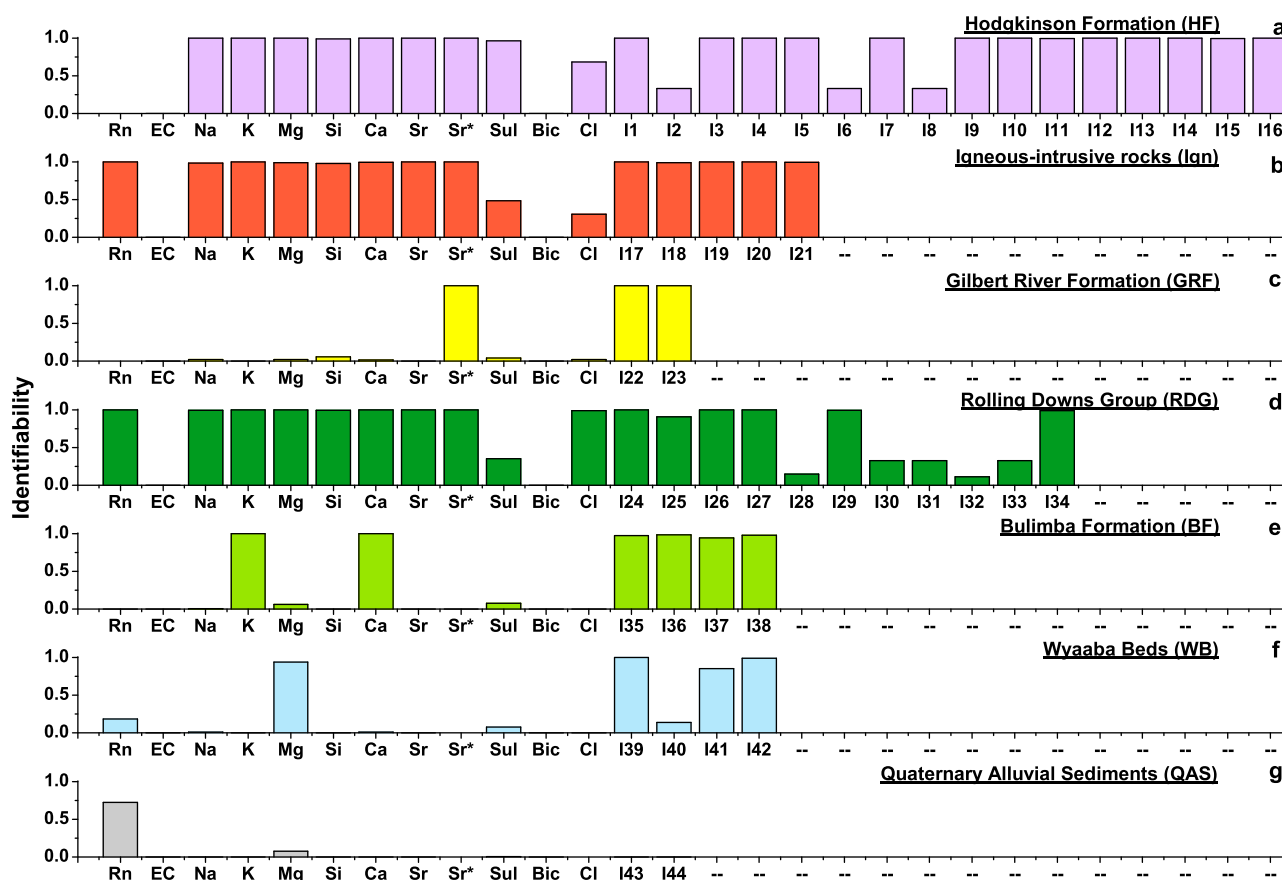
Figure 7. Model parameter identifiability for each geology formation (groundwater end-member): (a) Hodgkinson Formation; (b) Igneous-intrusive rocks; (c) Gilbert River Formation; (d) Rolling Downs Group; (e) Bulimba Formation; (f) Wyaaba Beds; (g) Quaternary Alluvial Sediments. Identifiability can vary between 0 and 1, the latter indicating complete identifiability (the parameter lies in the calibration solution space). Parameters: I: groundwater inflow (discharge zone); Rn, radon-222; EC, electrical conductivity; Sr, strontium; Sr*, strontium × $^{87}Sr/^{86}Sr$; Na, sodium; Ca, calcium; K, potassium; Mg, magnesium; Si, silicon; Cl, chloride; Sul, SO_4^{2-}; Bic, HCO_3^-.

The charge balance for modeled concentrations of major cations (Na^+, Ca^{2+}, K^+, and Mg^{2+}) and anions (HCO_3^-, SO_4^{2-}, and Cl^-) in groundwater discharge for each of the seven geologic units was consistently low, ranging from 2% to 5% (Figure S2a). With the exception of the Hodgkinson Formation, the modeled Σ[cations] (or Σ[anions]) in meq L^{-1} and modeled EC maintain a relationship of 1:100 (Figure S2b), indicating that modeled chemistry results are charge balanced and the proportionality between modeled EC and chemistry is maintained [*Appelo and Postma*, 2007].

The error associated with modeled groundwater discharge and its chemistry is shown in Figure 6 (right) as the 95% confidence interval for the estimated value. The confidence intervals provide a useful, visual, tool for comparing the associated uncertainty of modeled values. Calculated errors are consistently low for chemistry in the river sections where HF, Ign, and RDG formations outcrop. In contrast, errors are notably higher for the GRF, BF, WB, and QAS. Errors associated with estimating $^{87}Sr/^{86}Sr$ ratios are not available as the ratio is indirectly obtained from separately calibrated concentrations of Sr and Sr*, each with high R^2 (0.981 and 0.978, respectively) and low RMSE (0.0065 and 0.0053 mg L^{-1}, respectively).

4.6. Parameter Identifiability
The identifiability of each parameter is shown in Figure 7 for each geologic unit. Three out of seven geologic units, Hodgkinson Formation (HF), Igneous-intrusive (Ign), and Rolling Downs Group (RDG), are characterized by high identifiabilities in most of the modeled parameters. This result coheres with the low predictive errors computed for groundwater discharging in those sections where the Mitchell River flows across HF, Ign, and RDG geologic units. Similarly, identifiabilities were generally low and predictive errors in groundwater chemistry were generally higher for those sections corresponding to GRF, BF, WB, and QAS (Figure 6, right).
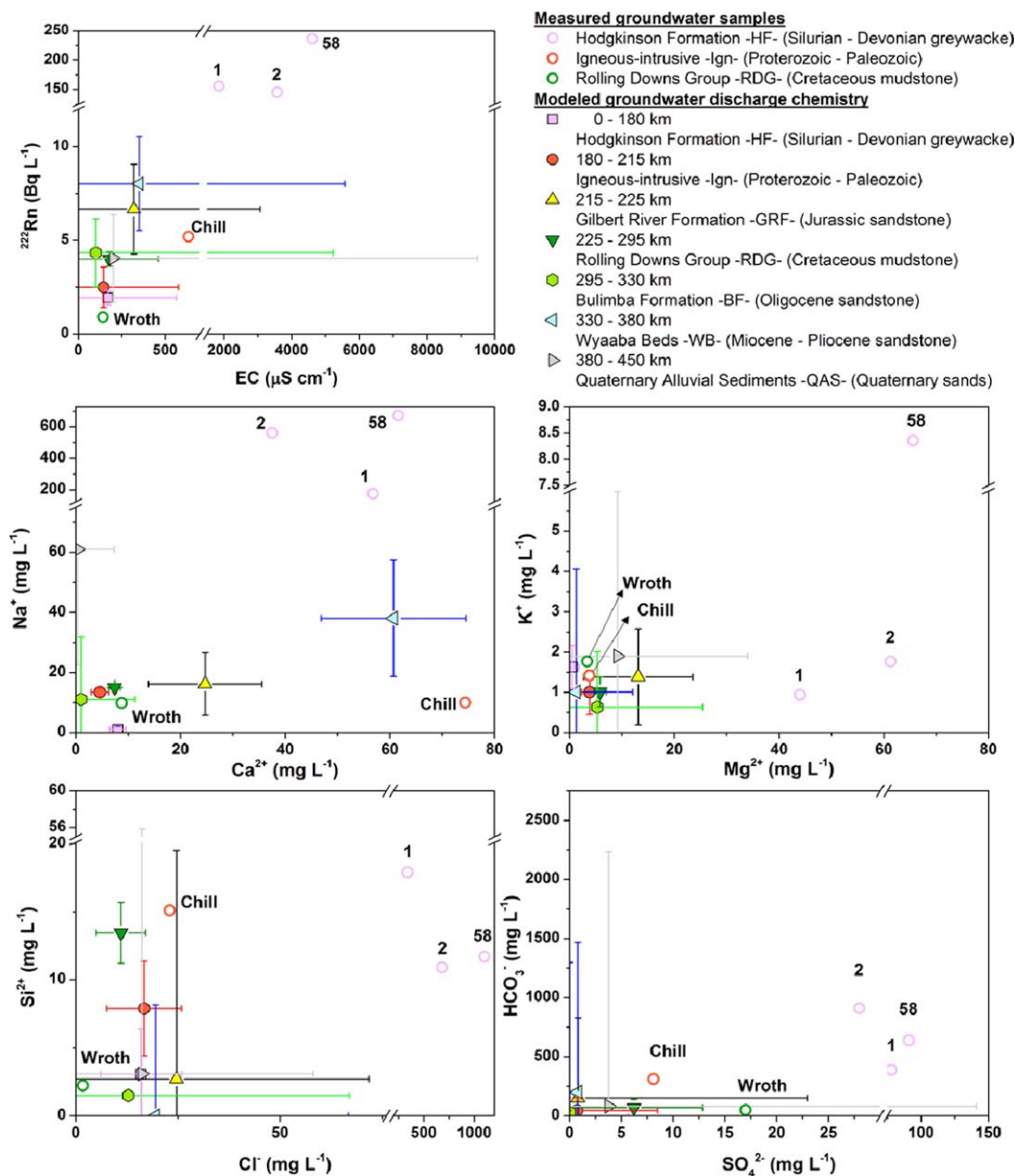
Figure 8. Modeled and measured chemical composition of groundwater discharge for each reach of geology (dots) and regional well samples (circles), respectively. Modeled error bars represent the 95% confidence interval for the estimated value from PEST, highlighting useful information on reliability of the estimated value.

Following *Doherty and Hunt* [2009], a qualitative identifiability level of 0.8 can be arbitrarily defined in order to mark the cutoff between parameters classed as identifiable and nonidentifiable. In this case, a total of 62 parameters out of 128 are classed as identifiable, 33 of which are groundwater inflow (Figure 7). The vast majority of these 62 parameters correspond to the three geologic units previously mentioned, HF, Ign, and RDG.

The low identifiabilities corresponding to groundwater discharge zones located in the BF, WB, QAS, and GRF appear to be independent of the location of the flow gauging stations and flow measurement points, as these are spatially well distributed along the entire length of the studied river section.

4.6. Source of Groundwater Inflow
The groundwater chemistry measured in five regional wells was compared to model-derived groundwater discharge chemistry (Figure 8). Measured groundwater chemistry from wells falls into two distinctive

groups. The first group of wells (1, 2, and 58), located in the HF geologic unit, are chemically distinct from the modeled groundwater discharging into the river in this area. All of these wells fall in the top right corner of the graphs, indicating comparatively high concentrations for all the measured parameters. Conversely, groundwater chemistry from the second group of wells (Chill and Wroth) has low concentrations for most of the parameters (except Ca^{2+} in Chill), similar to the modeled groundwater chemistry discharging from 180 km downstream. In terms of ion ratio, wells Chill and Wroth have quite similar ratios to modeled groundwater discharge, with 6 out of 10 parameters within the same order of magnitude. Modeled ratios overestimated between 8% and 40% for Mg/K and Cl/Si ratios, and the rest of modeled ratios underestimated by between 30% and 50%. The single exception was the overestimation of the Mg/K ratio for the RDG river reach by up to 200%. Modeled ion ratios of wells 1, 2, and 58 are consistently underestimated by 95%, while strongly overestimated for Ca/Na and Ec/Rn (up to 400% and over; Figure 8).

The modeled groundwater discharge for the reach where the RDG and Ign outcrops has consistently low errors, and ion ratios are relatively close to ratios measured in Wroth and Chill wells, respectively. For the RDG outcrop reach, ^{222}Rn activities, Na^+, Ca^{2+}, K^+, Mg^{2+}, and HCO_3^- concentrations and EC values are particularly close, indicating a direct connection between this geologic unit and groundwater discharge in this part of the catchment. Interestingly, 40% of the total groundwater discharge in the river occurs in this section.

Modeled ion ratios in the first 180 km (HF outcrops) do not match with ratios from regional groundwater sampled from wells 1, 2, and 58, which are completed and screened in the HF. Additionally, the only point that does not fall on or near the 1:100 line in Figure S2 corresponds to the modeled Σ[cations] of groundwater discharging in this area. Not surprisingly, this area of the catchment, and more precisely between 68 and 167 km, is where the flow event occurred. However, continuous monitoring of river water electrical conductivity showed <1% variation at 30 km downstream during the sampled period (C. Welsh, unpublished data, 2011). An analysis of the impact of the passage of the flood wave on river chemistry and estimates of groundwater discharge and its chemistry when applying a steady state model during transient river conditions revealed that a maximum overestimation of up to 75% is likely to occur during the first 100 km of a flow event similar to the one recorded during the sampling period (Appendix A and Figure A1). This error dramatically decreases if the sampling is performed after the peak of the flow event has passed. A close look at Figure 3 confirms that river sampling was performed after the peak of the flow event.

Interestingly, model calibration results consistently produced low errors for groundwater chemistry discharging in the HF outcrop area (Figure 6, right), despite the flow event recorded between 68 and 167 km. Although this might appear contradictory with the flow event and dissimilarity between modeled and measured ion ratios in this part of the catchment, it is rather elucidating. Low model calibration errors, together with high model identifiabilities, indicate that the chemistry of groundwater discharging to this river reach is quite distinctive, rather than being a mixture of many different sources. Local alluvial aquifers found in this part of the catchment, bank storage return or local recharge appear thus to be the main plausible sources of groundwater discharge, and likely one of them has stronger impact on groundwater discharge chemistry than the others.

5. Discussion and Conclusions

In this paper, we have shown that regional-scale sampling of river water chemistry can be used to infer spatial variations in the chemistry of groundwater discharging into a river. In practice, discharging groundwater will always be a mixture of water derived from many sources, including local aquifers, bank storage that was emplaced during previous river flow events, and in some cases regional aquifers [*McCallum et al.*, 2010, *Doble et al.*, 2012]. Hence, the methodology does not necessarily produce chemical compositions that represent the chemistry of groundwater sampled from regional wells. Rather, the concentration of groundwater discharge to the river may be intermediate between groundwater (either local or regional), bank storage return, and local recharge. If groundwater is much saltier than river water, ion ratios of discharge water should represent those of groundwater; on the contrary, if groundwater is fresh, ion ratios of discharge water should be representative of a mixture between groundwater, bank storage return, and local recharge.

It must be recognized that not all modeled parameters are equally identifiable. Although high identifiabilities are expected to relate to those parameters with low predictive errors, this is not a general rule. For

example, in this study identifiabilites for EC and HCO$_3^-$ (Bicarbonate, Bic) are zero for all geologic units, whereas low predictive errors were found for these parameters in three geologic units. This apparent contradiction occurs when two sensitive parameters are correlated. In these conditions, only the ratio of the correlated parameters and not the absolute value is sensitive to model results [*Haitjema*, 2006]. In this study, the combination of low predictive errors and high identifiabilities appeared to correspond to groundwater discharge with very distinctive chemistry, either regionally derived or bank storage return flow. Thus, it appears that the method, complemented with model uncertainty techniques, has potential to differentiate between local (e.g., bank storage) and regional groundwater sources discharging into the river using model uncertainty techniques.

Determining groundwater discharge rate, location, and chemistry from river sampling will be particularly accurate under nearly steady state, low river flow conditions. The method will still be valuable under transient conditions created by a flow event, particularly if river sampling is performed in a short period of time, after the passage of the flow wave and conservative tracers are targeted. In the case of the Mitchell River, we estimated that errors in the modeled major ion concentrations and other nongaseous tracers due to the flow wave may be 75% at the maximum (Figure A1). One important corollary of this finding is that all such tracers should have the same error, and thus estimated ratios of major ion concentrations will not be affected. Conversely, ion ratios of nonconservative tracers will not be maintained, which will be exacerbated if river sampling is performed just before or during the flow wave peak. Although we used a simplified approach to determine the impact of applying a steady state model to transient conditions created by a small flow event when determining groundwater discharge location and chemistry from river sampling, this is a promising contribution toward what we believe should be used in these situations: 3-D fully coupled surface water–groundwater models at the catchment scale.

Synoptic sampling of river water to infer groundwater chemistry is a promising technique to be considered for broad application to water management and environmental issues. Surface water contamination may be due to human activities (point and diffuse source) but often has its source in the geology of the catchment, either as heavy metals or salinity resulting from rock weathering. The link between catchment geology and river chemistry has previously been shown [*Bluth and Kump*, 1994], as well as the usefulness of synoptic sampling to determine mining impacts in surface water catchments [*Banks and Palumbo-Roe*, 2010]. The method we have presented is particularly useful for situations where management decisions need to be taken to mitigate the input of a contaminant load in the river system. For example, in an area where the primary water consumption is surface water, locating the source area of contaminants within the catchment can help to assess capture and treatment options before it enters the system. Also, it may help to allocate areas of water extraction and consumption without affecting the base flow and ecological status of the river. For example, our study identified that 40% of groundwater discharge occurred over only 15% of the river length.

The method is particularly useful for very remote areas where there are few wells available for sampling groundwater. While sampling remote catchments is challenging and may require sophisticated sampling techniques (e.g., helicopter), the method may be easily and routinely deployed for short river lengths where river access is possible. The method can be complemented with sampling groundwater prior its discharge to the river where possible, by installing drive points in the riverbed for example.

Appendix A: Impact of Nonsteady River Discharge

Equations (1) and (2) assume steady state river flow conditions, which are never absolutely achieved in reality. Transience can result in changes in river chemistry due to the passage of the flood wave, and changes in the chemistry of groundwater discharge due to near-stream mixing between river and groundwater. As our objective is to infer the chemistry of groundwater discharge from chemistry measured in the river, we have analyzed the impact of applying a steady state model to transient conditions created by a small flow event using a one-dimensional longitudinal river model with the fully coupled numerical code HydroGeoSphere [*Therrien et al.*, 2006]. The model dimensions represented, in a simplified form, the Mitchell River, with 450 km length, 20 m width, and 0.4 m water depth. For the purpose of this simulation, we assumed constant groundwater discharge (I_{gw}) of 0.3 m^3 d^{-1} m^{-1}, a rate close to the average groundwater discharge
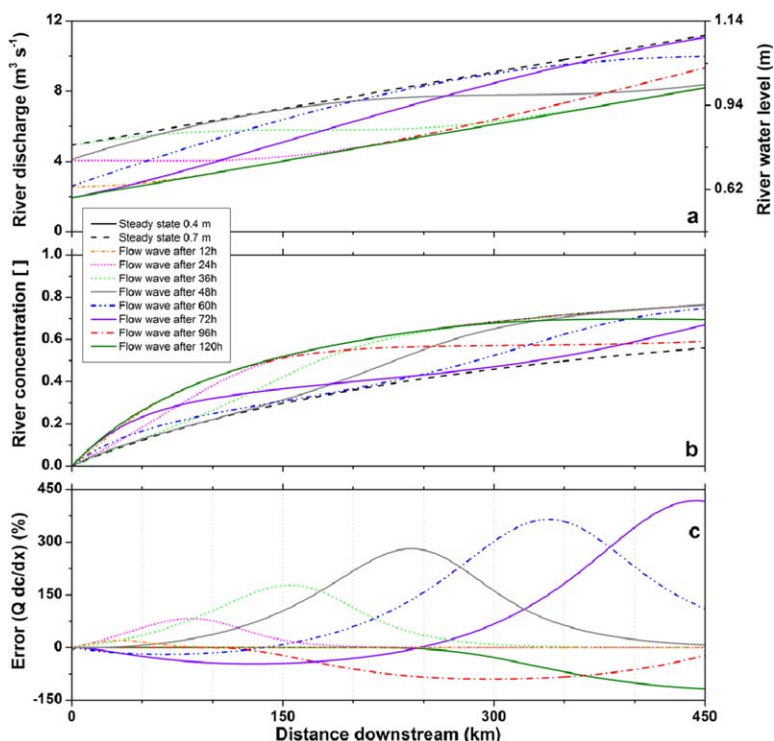
Figure A1. (a) River discharge and water level (b) and river concentration at two steady state water levels (0.4 and 0.7 m) and during a flow wave (0.3 m amplitude, 3 day period) at different times. (c) Error on groundwater discharge and concentration from an original steady state river water level of 0.4 m, caused by a small flow wave (0.3 m amplitude, 3 day period). Positive and negative errors indicate overestimation and underestimation rates, respectively, relative to the original steady state of 0.4 m.

along the first 180 km of the Mitchell River. Groundwater discharge concentration (C_{gw}) was assumed constant and equal to 1 (dimensionless) along the river length, while the surface water concentration at the upper boundary was set equal to zero ($C_{riv} = 0$; dimensionless). This approach does not model groundwater flow; it only solves river flow through the 1-D diffusion approximation of the Saint Venant equations and simulates solute transport in the river with the advection-dispersion equation. A cosine-shaped wave of similar characteristics to the measured one (0.3 m amplitude and period of 3 days, Figure 3) was modeled, and changes in river concentration recorded. Complete consideration of the combined effects of the passage of a flood wave and simultaneous exchange between river and groundwater would require a fully coupled 3-D groundwater-surface water model and extensive data collection, which is beyond the scope of this paper. Although the 1-D model used does not consider transience in groundwater discharge chemistry or rate caused by processes such as bank storage, it enables analysis of the influence of the propagation of a flow wave on river chemistry as a function of sampling time and distance downstream. In doing so it takes an important step forward toward assessing the impacts of using steady state models to represent transient systems.

Results of the theoretical HydroGeoSphere modeling analysis show how river water level (or discharge) and river concentrations at different times are enveloped within two steady states, prior to the flow event (0.4 m), and a steady state at 0.7 m (corresponding to an initial water level of 0.4 m plus a flood wave of amplitude equal to 0.3 m) (Figures A1a and A1b). According to Equation (2), for a conservative solute the groundwater discharge is approximately proportional to $Q\partial c/\partial x$. The divergence or error of $Q\partial c/\partial x$ from steady state is presented in Figure A1c for different times. As the wave of the flow event travels downstream, $Q\partial c/\partial x$ is likely to be overestimated by up to 400% 120 h after the start of the flow event, at a distance of 450 km. On the contrary, 12 h after the beginning of the flow event, $Q\partial c/\partial x$ is overestimated a maximum of 25% at 30 km downstream. The error in tracer concentration and groundwater discharge induced by flow wave propagation applies equally to any conservative tracer. Consequently, major ion ratios can still be resolved with minimal error if river samples are collected during transient flow conditions.

Modeling results from the steady state model indicated that important river losses occur at approximately 176 km, downstream of OK Bridge gauging station (167.3 km). The area is very remote; it is therefore considered unlikely that this loss can be attributed to extraction by pumping from the river. The flow event seems to dissipate between OK Bridge (167.3 km) and Gamboola (257.0 km) gauging stations, and it is likely that the 24% increase in discharge at Gamboola between the 16 and the 17 October is mostly due to the increase in discharge of the Walsh River (19% as measured at Trimbles Crossing). Given the important loss rate at 176 km (2.8×10^5 m^3 d^{-1}) and the small size of the flow event, it is speculated that the event did not travel further than this point, limiting the effect of the flow event to 100 km, between 68 and 167 km. According to model results presented in Figure A1, a maximum overestimation of the groundwater discharge and its chemistry of 75% will occur in the first 100 km 36 h after the beginning of a flow event. Overestimation dramatically decreases after the peak of the flow wave has passed. River sampling was performed after the flow wave peak (Figure 3), confirming modeled groundwater discharge and chemistry using the 1-D steady state model might have been overestimated by 75%, in the worst case scenario, between 68 and 167 km downstream.

References

Appelo, C. A. J., and D. Postma (2007), *Geochemistry, Groundwater and Pollution*, 2nd ed., 649 pp., A. A. Balkema, Amsterdam, Netherlands.

Banks, V. J., and B. Palumbo-Roe (2010), Synoptic monitoring as an approach to discriminating between point and diffuse source contributions to zinc loads in mining impacted catchments, *J. Environ. Monit.*, *12*(9), 1684–1698.

Barringer, J. L., J. L. Bonin, M. J. Deluca, T. Romagna, K. Cenno, M. Alebus, T. Kratzer, and B. Hirst (2007), Sources and temporal dynamics of arsenic in a New Jersey watershed, USA, *Sci. Total Environ.*, *379*(1), 56–74.

Blum, J. D., Y. Erel, and K. Brown (1993), ^{87}Sr/^{86}Sr ratios of sierra nevada stream waters: Implications for relative mineral weathering rates, *Geochim. Cosmochim. Acta*, *57*(21–22), 5019–5025.

Bluth, G. J. S., and L. R. Kump (1994), Lithologic and climatologic controls of river chemistry, *Geochim. Cosmochim. Acta*, *58*(10), 2341–2359.

Burke, W. H., R. E. Denison, E. A. Hetherington, R. B. Koepnick, H. F. Nelson, and J. B. Otto (1982), Variation of seawater ^{87}Sr/^{86}Sr throughout Phanerozoic time, *Geology*, *10*(10), 516–519.

Cook, P. G., G. Favreau, J. C. Dighton, and S. Tickell (2003), Determining natural groundwater influx to a tropical river using radon, chlorofluorocarbons and ionic environmental tracers, *J. Hydrol.*, *277*, 74–88.

Cook, P. G., S. Lamontagne, D. Berhane, and J. F. Clark (2006), Quantifying groundwater discharge to Cockburn River, southeastern Australia, using dissolved gas tracers ^{222}Rn and SF$_6$, *Water Resour. Res.*, *42*, W10411, doi:10.1029/2006WR004921.

CSIRO (2009), Water in the Mitchell region, in *Water in the Gulf of Carpentaria Drainage Division, Reports to the Australian Government from the CSIRO Northern Australia Sustainable Yields Project*, pp. 347–416, CSIRO Water for a Healthy Country Flagship, Australia.

Doble, R., P. Brunner, J. McCallum, and P. G. Cook (2012), An analysis of river bank slope and unsaturated flow effects on bank storage, *Ground Water*, *50*(1), 77–86.

Doherty, J. (2008), PEST *Model-Independent Parameter Estimation. User Manual and Addendum*, Watermark Numer. Comput., 336 pp., Brisbane, Australia.

Doherty, J., and R. J. Hunt (2009), Two statistics for evaluating parameter identifiability and error reduction, *J. Hydrol.*, *366*, 119–127.

Doherty, J., and R. J. Hunt (2010), Approaches to highly parameterized inversion: A guide to using PEST for groundwater-model calibration, *U.S. Geol. Surv. Sci. Invest. Rep. 2010–5169*, 59 pp.

Ellins, K. K., A. Roman-Mas, and R. Lee (1990), Using ^{222}Rn to examine groundwater/surface discharge interaction in the Rio Grande de Manati, Puerto Rico, *J. Hydrol.*, *115*, 319–341.

Gardner, W. P., G. A. Harrington, D. K. Solomon, and P. G. Cook (2011), Using terrigenic ^{4}He to identify and quantify regional groundwater discharge to streams, *Water Resour. Res.*, *47*, W06523, doi:10.1029/2010WR010276.

Gehrke, P., et al. (2004), Sustainable futures for Australia's tropical rivers—A strategy for developing research directions for Australia's tropical river systems, *Tech. Rep. 17/04*, 19 pp., CSIRO Land and Water, Darwin, Australia.

Haitjema, H. (2006), The role of hand calculations in ground water flow modeling, *Ground Water*, *44*(6), 786–791.

Harrington, G. A., and A. L. Herczeg (2003), The importance of silicate weathering of a sedimentary aquifer in arid Central Australia indicated by very high ^{87}Sr/^{86}Sr ratios, *Chem. Geol.*, *199*(3–4), 281–292.

Harrington, G. A., W. P. Gardner, and T. Munday (2013), Tracking groundwater discharge to a large river using tracers and geophysics, *Ground Water*, doi: 10.1111/gwat.12124, in press.

Holtzman, R., U. Shavit, M. Segal-Rozenhaimer, I. Gavrieli, A. Marei, E. Farber, and A. Vengosh (2005), Quantifying ground water inputs along the Lower Jordan River, *J. Environ. Qual.*, *34*(3), 897–906.

Kimball, B. K., R. R. Runkel, and L. G. Gerner (2001), Quantification of mine-drainage inflows to Little Cottonwood Creek, Utah, using a tracer-injection and synoptic-sampling study, *Environ. Geol.*, *40*(11), 1390–1404.

Leaney, F. W., and A. L. Herczeg (2006), A rapid field extraction method for determination of radon-222 in natural waters by liquid scintillation counting, *Limnol. Oceanogr. Methods*, *4*, 254–259.

McCallum, J. L., P. G. Cook, P. Brunner, and D. Berhane (2010), Solute dynamics during bank storage flows and implications for chemical base flow separation, *Water Resour. Res.*, *46*, W07541, doi:10.1029/2009WR008539.

McGuire, K. J., J. J. McDonnell, M. Weiler, C. Kendall, B. L. McGlynn, J. M. Welker, and J. Seibert (2005), The role of topography on catchment-scale water residence time, *Water Resour. Res.*, *41*, W05002, doi:10.1029/2004WR003657.

McNutt, R. H. (1999), Strontium isotopes, in *Environmental Tracers in Subsurface Hydrology*, edited by P. Cook and L. Herczeg, pp. 233–260, Kluwer Acad., Norwell, Mass.

Meredith, K. T., S. E. Hollins, C. E. Hughes, D. I. Cendón, S. Hankin, and D. J. M. Stone (2009), Temporal variation in stable isotopes (^{18}O and ^{2}H) and major ion concentrations within the Darling River between Bourke and Wilcannia due to variable flows, saline groundwater influx and evaporation, *J. Hydrol.*, *378*, 313–324.

Négrel, P., and P. Deschamps (1996), Natural and anthropogenic budgets of a small watershed in the massif central (France): Chemical and strontium isotopic characterization of water and sediments, *Aquat. Geochem.*, *2*(1), 1–27.

Négrel, P., and P. Lachassagne (2000), Geochemistry of the Maroni River (French Guiana) during the low water stage: Implications for water–rock interaction and groundwater characteristics, *J. Hydrol.*, *237*, 212–233.

Opsahl, S. P., S. E. Chapal, D. W. Hicks, and C. K. Wheeler (2007), Evaluation of ground-water and surface-water exchanges using streamflow difference analyses, *J. Am. Water Resour. Assoc.*, *43*(5), 1132–1141.

Peeters, L. J. M., D. Rassam, and J. Lerat (2011), Improving parameter estimation in transient groundwater model through temporal differencing, *MODSIM2011, 19th International Congress on Modelling and Simulation, Modelling and Simulation Society of Australia and New Zealand*, edited by F. Chan, D. Marinova, and R. S. Anderssen, pp. 3959–3965, Dec.

Petelet, E., J.-M. Luck, D. Ben Othman, P. Negrel, and L. Aquilina (1998), Geochemistry and water dynamics of a medium-sized watershed: The Hérault, southern France: 1. Organisation of the different water reservoirs as constrained by Sr isotopes, major, and trace elements, *Chem. Geol.*, *150*(1–2), 63–83.

Petelet-Giraud, E., P. Négrel, and J. Casanova (2003), Variability of $^{87}Sr/^{86}Sr$ in water draining granite revealed after a double correction for atmospheric and anthropogenic inputs, *Hydrol. Sci. J.*, *48*(5), 729–742.

Petelet-Giraud, E., P. Négrel, L. Gourcy, C. Schmidt, and M. Schirmer (2007), Geochemical and isotopic constraints on groundwater-surface water interactions in a highly antrhopized site. The Wolfen/Bitterfeld megasite (Mulde subcatchment, Germany), *Environ. Pollut.*, *148*, 707–717.

Reeder, S. W., B. Hitchon, and A. A. Levinson (1972), Hydrogeochemistry of the surface waters of the Mackenzie River drainage basin, Canada—I. Factors controlling inorganic composition, *Geochim. Cosmochim. Acta*, *36*(8), 825–865.

Séguis, L., et al. (2011), Origins of streamflow in a crystalline basement catchment in a sub-humid Sudanian zone: The Donga basin (Benin, West Africa): Inter-annual variability of water budget, *J. Hydrol.*, *402*, 1–13.

Semhi, K., N. Clauer, and J.-L. Probst (2000), Strontium isotope compositions of river water as records of lithology-dependent mass transfers: The Garonne river and its tributaries (SW France), *Chem. Geol.*, *168*, 173–193.

Smerdon, B. D., W. Payton Gardner, G. A. Harrington, and S. J. Tickell (2012), Identifying the contribution of regional groundwater to the baseflow of a tropical river (Daly River, Australia), *J. Hydrol.*, *464–465*, 107–115.

Stallard, R. F., and J. M. Edmond (1983), Geochemistry of the Amazon: 2. The influence of geology and weathering environment on the dissolved load, *J. Geophys. Res.*, *88*(C14), 9671–9688.

Therrien, R., R. G. McLaren, E. A. Sudicky, and S. M. Panday (2006), HydroGeoSphere, Groundwater Simul. Group, Univ. of Waterloo, Waterloo, Ont., Canada.

Webster, I. T., N. Rea, A. V. Padovan, P. Dostine, S. A. Townsend, and S. Cook (2005), An analysis of primary production in the Daly River, a relatively unimpacted tropical river in northern Australia, *Mar. Freshwater Res.*, *56*(3), 303–316.